Journal of Materials Chemistry B

Surfaces with Antifouling-Antimicrobial Dual Function via Immobilization of Lysozyme on Zwitterionic Polymer Thin Films

Journal:	*Journal of Materials Chemistry B*
Manuscript ID	TB-ART-11-2021-002597.R2
Article Type:	Paper
Date Submitted by the Author:	29-Jan-2022
Complete List of Authors:	Khlyustova, Alexandra ; Cornell University, Robert F. Smith School of Chemical and Biomolecular Engineering Kirsch, Mia; Cornell University, Robert F. Smith School of Chemical and Biomolecular Engineering Ma, Xiaojing; Cornell University, Robert F. Smith School of Chemical and Biomolecular Engineering Ithaca, NY, USA Cheng, Yifan; Cornell University, Robert F. Smith School of Chemical and Biomolecular Engineering Yang, Rong; Cornell University, Robert F. Smith School of Chemical and Biomolecular Engineering

Surfaces with Antifouling-Antimicrobial Dual Function via Immobilization of Lysozyme on Zwitterionic Polymer Thin Films

Alexandra Khlyustova, Mia Kirsch, Xiaojing Ma, Yifan Cheng and Rong Yang*

Robert F. Smith School of Chemical & Biomolecular Engineering

Cornell University, Ithaca, New York, 14853, USA.

* Corresponding Author Contact: ryang@cornell.edu

Abstract

Due to the emergence of wide-spread infectious diseases, there is a heightened need for antimicrobial and/or antifouling coatings that can be used to prevent infection and transmission in a variety of applications, ranging from healthcare devices to public facilities. While antimicrobial coatings kill pathogenic bacteria upon contact with the surface, the antimicrobial function alone often lacks long-term effectiveness due to the accumulation of dead cells and their debris on the surface, thus reducing performance of the coating overtime. Therefore, it is desirable to develop coatings with the dual functions of antimicrobial efficacy and fouling resistance, where antifouling coatings afford the added benefit of preventing the adhesion of dead cells and debris. Leveraging the outstanding antifouling properties of zwitterionic coatings, we synthesized copolymers with antimicrobial-antifouling dual function by immobilizing lysozyme, a common antimicrobial enzyme, to the surface of a pyridinium-based zwitterionic copolymer. Specifically, poly(4-vinylpyridine-*co*-pentaflurophenyl methacrylate-*co*-divinyl benzene) [P(4VP-PFPMA-DVB)] thin films were synthesized by an all-dry vapor deposition technique, *initiated* Chemical Vapor Deposition, and derivatized using 1,3-propanesultone to obtain sulfobetaine moieties. Lysozyme, known to hydrolyze polysaccharides in the cell wall of gram-positive bacteria, was immobilized by forming amide bonds with the copolymer coating via nucleophilic substitution of the pentafluorophenyl group. The antifouling and antibacterial performance of the novel lysozyme-zwitterionic coating was tested against gram-positive *Bacillus subtilis* and gram-negative *Pseudomonas aeruginosa*. A reduction of surface adhesion of 87% was achieved for *P. aeruginosa*, and of 75% for *B. subtilis* when compared to a common poly(vinyl chloride) surface. The lysozyme-zwitterionic coating also deactivated 67% of surface-attached gram-positive bacteria, *B. subtilis*. This novel dual-function material can

produce anti-infection surfaces for medical devices and surgical tools, personal care products, and surfaces in public facilities.

Keywords: zwitterionic, antifouling, antimicrobial, polymer, enzyme, immobilization, functionalization, deposition.

1. Introduction

Recent years have witnessed an increasing number of hospital-acquired infections caused by pathogen-contaminated surfaces[1] calling for accelerated development of novel biomaterials to prevent fomite transmissions. Antimicrobial coatings have been developed to diminish the spread of pathogens by deactivating bacteria upon surface contact,[2] which have been used in a range of applications such as medical instruments, food packaging, and implantable devices.[3] For example, poly(dimethyl amino methyl styrene) [PDMAMS] thin films led to over 99.9% eradication of *E. coli* and *B. subtilis* after 1 hour of incubation.[4] Coating of 3-(4′-vinylbenzyl)-5,5-dimethylhydantoin (VBDMH), synthesized by admicellar polymerization, showed deactivation of 99.98% *S. aureus* and 99.94% *E. coli* within 1-30 minutes.[5] Immobilization of lysozyme, an enzyme that hydrolyzes polysaccharides in the cell wall of gram-positive bacteria, was also proven effective as an antimicrobial surface design.[6] Previously, ethylene vinyl alcohol films were immobilized with lysozyme and showed eradication of 80% of the surface-adhered *Listeria monocytogenes*;[7] immobilization of lysozyme on cellulose nanofibers achieved deactivation rates of roughly 70%, 35%, 46%, and 78% against *S. aureus, E. coli, L. monocytogenes*, and *S. cerevisiae*, respectively.[8] Furthermore, lysozyme is known for its excellent anti-inflammatory properties,[9] as well as antiviral efficacies in a few reports.[10,11]

Although antimicrobial surfaces are fast acting, their long-term effectiveness has been limited due to the accumulation of dead cells and their debris on the surface and thus loss of direct contact between pathogens and the antimicrobial moieties (e.g., amine or lysozyme).[12] The adhered cells and debris could further serve as a conditioning layer that promotes downstream formation of biofilms, exacerbating infectious diseases and potentially leading to long-term infections.[13] For example, robust antimicrobial coatings that contain silver and ruthenium still

suffered from the biofilm formed by *Staphylococcus aureus*, which was as much as 54% in volume density compared to sterile cover slips.[14] Therefore, prevention of fomite transmission of infectious diseases calls for surface coatings that demonstrate strong antibacterial efficiency and fouling resistance simultaneously.

Antifouling coatings consist primarily of hydrophilic materials, which are known to reduce attachment of bacteria through a strong hydration layer (the enthalpic effect) and/or the compression of polymer chains (the entropic effect).[15] Over the past decade, zwitterionic materials have made substantial impact in the field of antifouling materials design due to their outstanding fouling resistance[16] and biocompatibility.[17] Zwitterionic materials have equal parts of cationic and anionic groups with an overall neutral charge,[18] and are often super-hydrophilic due to the strong hydration layer.[19] For example, poly(sulfobetaine) (pSB)[20] has demonstrated an ultralow level of nonspecific protein adsorption,[21] bacterial adhesion,[22] and biofilm formation.[23] Hence, zwitterionic materials have been used in a wide range of biological and medical applications, including antibiofouling coatings for biomedical devices,[24] efficient drug nanocarriers,[25] biocompatible tissue scaffolds,[26] and stabilizer for enzymes. [27]

Traditionally, antimicrobial/antifouling mono-functional polymers are synthesized via free radical polymerization, anionic polymerization, group transfer polymerization, or reverse addition-fragmentation chain-transfer (RAFT) polymerization.[18] However, these solution-based methods often have limitations that stem from the requirement of large amounts of organic solvents during polymer synthesis and application.[28] For instance, harmful solvents like dimethylformamide (DMF), tetrahydrofuran (THF), and dimethyl sulfoxide (DMSO) could reduce the biocompatibility of the resulting antimicrobial/antifouling polymers.[29] When applied as self-assembled monolayers (SAMs), the antimicrobial/antifouling polymers can only be

prepared on gold substrates.[30] To overcome these challenges, we report here the all-dry synthesis of a functionalizable zwitterionic polymer coating, which was subsequently reacted to immobilize lysozyme to enable antimicrobial-antifouling dual functions (Scheme 1). This three-step synthesis procedure reported here also has the added benefit of simplicity, especially compared to the existing methods used to synthesize dual-functional coatings that often comprise over a dozen steps.[13,31–34]

The all-dry polymerization was accomplished using *initiated* Chemical Vapor Deposition (iCVD),[35,36] which performs polymerization and coating application in a single step, giving rise to polymer thin films on virtually any substrate.[37] iCVD is an all-dry polymerization technique, which follows the free-radical chain-growth mechanism. iCVD enables synthesis of fully-polymerized thin films because all residual monomers are removed by vacuum degassing.[38] The room-temperature processing employed by iCVD (generally 15-50°C) also minimizes side reactions, resulting in ultra-high purity polymer thin films.[39] Using iCVD, we synthesized a functionalizable copolymer, poly(4-vinylpyridine-pentaflurophenyl methacrylate-divinyl benzene) [P(4VP-PFPMA-DVB)]. The comonomer, PFPMA, was chosen because of its pentafluorophenyl ester side chain, which is prone to nucleophilic substitution by primary-amine-containing molecules like enzymes,[40,41] hence enabling the immobilization of lysozyme. The iCVD technique uniquely allows the random copolymerization of the hydrophilic monomer, 4VP, and the hydrophobic monomer, PFPMA, thanks to its solvent-free nature. DVB was copolymerized with 4VP and PFPMA to prevent dissolution and enhance stability of the coating. Pyridinium-based sulfobetaine was obtained by derivatizing P(4VP-PFPMA-DVB) with 1,3-propane sultone (PS) in vapor-phase.[42] The subsequent immobilization of lysozyme onto the zwitterionic coating was achieved by incubating the coating with an aqueous solution of

lysozyme at 37°C. Successful immobilization was confirmed using scanning electronic microscopy (SEM), atomic force microscopy (AFM), and x-ray photoelectron spectroscopy (XPS). Finally, the antifouling-antimicrobial dual function of the novel coating was demonstrated using gram-positive *Bacillus subtilis* and gram-negative *Pseudomonas aeruginosa*, as evaluated by confocal microscopy.

2. Experimental

2.1 Materials

Pentafluorophenyl methacrylate (PFPMA) was purchased from Synquest Laboratories. Divinyl benzene (DVB, 80%), 4-vinylpyridine (4VP, ≥ 95%), 1,3-propane sultone (PS, 98%), *tert*-butyl peroxide (TBPO, 98%), trichlorovinylsilane (TCVS, 97%), sodium chloride (NaCl, ≥ 99%), and lysozyme solution (10 mg/mL) were acquired from Sigma Aldrich. Clear poly(vinyl chloride) [PVC] film was purchased from McMaster-Carr. Phosphate buffered saline (PBS) (20X, ultra-pure grade) was acquitted from VWR. PBS was diluted 1:20 with Milli-Q water to make PBS (1X) solution. The microscope cover slips (18 x 18 mm) were obtained from Fisher Scientific. Silicon (Si) wafer was purchased from Pure Wafer. 6-Well plates were acquired from Corning. The 35 mm confocal dishes with 15 mm glass bottom for imaging were purchased from VWR. For bacteria culture, lysogeny broth (LB, Difco) was used as a culture medium. Deionized water was produced by using a Milli-Q unit (Millipore) with a resistivity of 18.2 MΩ-cm at 25 ºC.

2.2 Polymer thin film synthesis using iCVD

Depositions were done on glass cover slips for subsequent bacterial culture and on silicon (Si) wafer for in-situ monitoring of coating thickness and material characterizations. Prior to deposition, the substrates were cleaned in a plasma cleaner (PDC-001-HP, Harrick Plasma)

under vacuum with pressure <100 mTorr. After plasma cleaning, the samples were immediately moved to a desiccator containing 1 mL TCVS, and a silane coupling reaction was performed under vacuum for 5 minutes to prevent the delamination of the copolymer thin films. Homopolymers of P4VP and PPFPMA and copolymers of P(4VP-PFPMA) and P(4VP-PFPMA-DVB) were deposited in the custom-made iCVD reactor. The polymerization reaction is depicted in Scheme 1a. Thermal decomposition of the TBPO was facilitated by the filament that was made of copper/chromium wires (80% Ni/ 20% Cr, Goodfellow), mounted parallel to each other in an array that was positioned ~2 cm above the reactor stage. The filament was heated to the temperature of 250°C by a DC power supply (B&K Precision). A cooling stage, on which the substrate to be coated was placed, was kept at 30°C by an Accel 500 LC chiller (Thermo Fisher). The reactor chamber temperature was set to 60°C. Temperatures of the filament, stage, and reactor chamber were monitored using type K thermocouples (Omega Engineering). The pressure of the reactor chamber was maintained at 0.25 Torr by a butterfly throttle valve (MKS Instruments). The polymer coating thickness on a Si wafer was monitored by *in- situ* laser interferometry (He-Ne laser, JDSU). During depositions, TBPO and Argon were kept at room temperature, and metered into the reactor through mass flow controllers (MKS Instruments). The monomers, i.e., 4VP, PFPMA, and DVB, were used without further purification, and were heated to 50°C, 50°C and 60°C, respectively, in glass jars and metered into the reactor through needle valves (Swagelok). The needle valves were maintained at the temperature of 80°C. The deposition conditions for the homopolymers and copolymers were summarized in Table 1. To ensure that polymer thin films were smooth and that there was no condensation on the stage, all samples were deposited with a total P_m/P_{sat} (i.e., the total fractional saturation pressure of all monomers used in a single deposition) to be less than 0.2. [43]

2.3 Formation of zwitterionic moieties via vapor-phase derivatization

The as-deposited thin films were fixed at the top of a crystallizing dish (VWR) with Kapton tape. 1 g of PS was added to the bottom of the dish. The dish was covered with aluminum foil and transferred into a vacuum oven (VivTek, FVL-A30) and incubated for 6 hours at 60ºC.[44] The schematic for the vapor-phase derivatization reaction is depicted in Scheme 1a. After the reaction, a sulfobetaine functional group was formed producing a zwitterionic form of the copolymer thin film, P(4VPz-PFPMA-DVB).[45]

2.4 Enzyme immobilization via nucleophilic substitution reaction

Following the vapor-phase derivatization, the coated glass cover slips and Si wafer were incubated in a lysozyme solution in PBS (1 mg/mL) for 6 hours at 37°C.[40] This temperature was selected to avoid denaturation of lysozyme, which has been reported to occur at above 40°C.[46] After incubation, the samples were rinsed with PBS and Milli-Q water and stored in PBS at 4°C prior to subsequent studies.

2.5 Thickness measurements of the polymer thin films

The coating thickness was measured on flat Si wafer using a J.A. Woollam Alpha-SE spectroscopic ellipsometer at three different incidence angles of 65°, 70°, and 75° with wavelength range from 315 to 718 nm.[35] The Cauchy-Urban model was used to fit the data.

2.6 Chemical characterization of the polymer thin films

Fourier transform infrared (FTIR) spectra were collected using a Nicolet iS50 (Thermo Fisher Scientific) spectrometer in transmission mode. The spectra were collected with a deuterated triglycine sulfate (DTGS) detector over the range of 500 – 4000 cm^{-1} with resolution of 4 cm^{-1}. The data was averaged over 128 scans to improve the signal-to-noise ratio.[47] All

collected spectra were normalized by the polymer film thickness and baseline-corrected by subtracting a background spectrum (Si wafer) using the OMNIC software.

Prior to XPS, all samples were stored in a vacuum box. XPS was done using a Scienta Omicron ESCA 2SR spectrometer with a monochromatized Al Kα source at a power of 150 W and voltage of 12 kV. The charge neutralizer was set to beam energy of 5 eV, focus voltage of 300 V and emission of 15 μA. The survey spectra were collected over 0 – 1200 eV, while N(1s) and C(1s) high resolution spectra were collected over 392 - 412 eV and 278 – 303 eV, respectively. The atomic percentage (at. %) of each element in the samples were determined by using CasaXPS software with Shirley background. The charging was corrected by using the reference value of 284.8 eV, which is the binding energy for C-C and C-H bonds arising in C(1s) high-resolution spectra.[48]

2.7 Dynamic contact angle evaluation on the polymer thin films

To determine contact angle hysteresis, dynamic water contact angles (WCA), i.e., advancing and receding contact angles, were measured by Rame-Hart Model 500 goniometer at room temperature with Milli-Q water using the volume-addition method. Water droplets were dispensed onto a surface by using an automatic dispenser. The advancing contact angle was defined to be the largest angle obtained on the surface when increasing the drop size from 1 µL to 10 µL while the receding angle was the smallest angle obtained during retraction of a water droplet from 10 µL to 0 µL.

2.8 Assessment of crystallinity of the polymer thin films

X-ray diffraction (XRD) was performed using a Bruker-D8 Power Diffractometer from 10 to 50° to measure the crystallinity of the samples.

2.9 Characterization of the film surface morphology

Surface morphology was evaluated by using AFM and SEM. Asylum-MFP3D-BIO microscope was utilized in AC tapping mode with n^+-Si PPP-NCSTR-10 cantilevers (Nanosensors). To quantify surface roughness, 5 x 5 μm regions of copolymer thin films (coated onto Si wafers) were scanned with a frequency of 0.5 Hz. Top-view SEM images of the polymer thin films were captured by Zeiss Gemini 500 microscope at electron beam energy of 1 eV. Prior to SEM imaging, the samples were coated with ~5 nm gold to prevent electron charging.

2.10 Evaluation of antifouling and antimicrobial performance

B. subtilis (DK1042 strain) and *P. aeruginosa* (PAO1 strain) were used for experimental validation of the antifouling-antimicrobial dual function. Those strains were selected because they were commonly used model strains in antifouling and antimicrobial research.[44,49] Both strains were preserved in glycerol at - 80°C prior to the validation experiments.

The assessment of dual function began with streaking out bacteria cells from the frozen stocks onto fresh trypticase soy agar (TSA) plates, and incubating them overnight (for ~16 hours) at 37°C. After the incubation, the plates were taken out and a single colony of each strain was inoculated in LB medium and cultured for 18 hours at 37°C in a shaker at 225 rpm. After 18 hours, OD_{600} measurements reached ~0.2 - 0.3 for DK1042 and ~0.5 - 0.6 for PAO1. Both overnight cultures were diluted 10 times for the antifouling-antimicrobial tests. Meanwhile, coated coverslips or PVC films were placed into a 6-well plate and disinfected under UV light for 30 minutes. 3 mL of the 10-time dilutions of the overnight cultures was added into each well, in which the coverslips and PVC films were incubated horizontally at 37°C for 2 hours to allow enough time for bacteria to interact with the surfaces. After the incubation, the coverslips and PVC films were removed from the 6-well plate and washed with 0.15 M solution of NaCl. The

cover slips were then stained using LIVE/DEAD BacLight Bacterial Viability Kit (Thermo Fisher) for 15 minutes, rinsed with NaCl solution, and then put onto a confocal dish for subsequent observation using a Zeiss 710 confocal microscope (40x water objective). The antifouling and antimicrobial performance was evaluated by counting the bacteria in fluorescent green (488 nm laser) and red (561 nm laser), respectively. The number of adhered cells was quantified using the Fiji/ImageJ software.

2.11 Evaluation of cytotoxicity

The primary human dermal fibroblast cells (HDF, ATCC PCS-201-012) were cultured using the Fibroblast Basal Medium (ATCC PCS-201-030) and the Fibroblast Growth Kit-Low Serum (ATCC PCS-201-041) in a humidified 5% CO_2-containing balanced-air incubator at 37°C.

Transwell membrane inserts (0.4-μm pore size; Costar, USA) and the 24-well plates (Corning Costar, USA) were used as the donor and acceptor chambers, respectively. The fibroblast cell was seeded at a density of 4×10^4 cells per well in a 24-well plate and incubated overnight at 37 °C in a humidified 5% CO_2-containing atmosphere. After that, the medium in each well was replaced by 1 mL fresh medium. The Transwell membrane insert containing a coverslip (5 mm*5 mm) with P(4VPz-PFPMA-DVB-lysozyme) was placed into the 24-well plate with the samples merged in fresh medium and co-incubated with the cells for 24 and 48 hours. The cells exposed to the clean glass coverslip were tested as a control group. Viability of the cells was quantified using the Cell Counting Kit-8 (CCK-8 kit; Dojindo Molecular Technologies, Japan). The absorbance at 450 nm was measured after incubating cells with the CCK-8 kit reagents for 1-2 hours. Empty wells with CCK-8 assay reagents only were used as blanks and their average absorbance was subtracted from the final reading. Relative cell viability

240 was calculated by normalizing the absorbance readings using that of untreated cells. All assays
241 were carried out in quadruplicates.

242 3. Results and Discussion

243 3.1 Synthesis and characterization of the copolymer P(4VP-PFPMA-DVB)

244 Copolymer P(4VP-PFPMA-DVB) and homopolymers of P4VP and PPFPMA were
245 synthesized via iCVD. DVB was used as a crosslinker to prevent coating dissolution during or
246 after the immobilization of lysozyme. The solvent-free nature of iCVD makes it attractive for
247 biomedical and biological applications, where toxic solvents are to be avoided if possible.[28] The
248 iCVD technique consists of three simultaneous processes: (1) decomposition of initiator, TBPO
249 in this case, upon passing resistively heated filament array to generate free radicals, (2)
250 adsorption of vaporized monomers onto a cooled substrate, and (3) chemisorption of free radicals
251 onto the monomer-covered substrate to initiate a polymerization reaction on the substrate and
252 form a thin film.[50,51] Coating thickness was monitored in real time using a laser interferometer
253 and polymer growth was terminated once the desirable thickness (~100 nm) was reached.
254 Pyridinium-based sulfobetaine side groups were formed via the vapor-phase reaction with PS
255 under vacuum.

256 Molecular structures of P4VP, PPFPMA, P(4VP-PFPMA), and P(4VP-PFPMA-DVB)
257 that were synthesized using the iCVD technique were first confirmed using FTIR (Figure 1a).
258 The thickness-normalized P4VP spectrum had peaks at 1597 cm^{-1} and 1416 cm^{-1}, which were
259 characteristic vibrations of the pyridine ring. The FTIR spectrum of PPFPMA had 4
260 characteristic peaks. The strongest peak was located at 1520 cm^{-1}, which corresponded to the
261 vibration of C-C in the benzene ring. The peaks at 1065 cm^{-1} and 995 cm^{-1} were due to the ester
262 bond and the C-F moiety, respectively. The absorption at 1780 cm^{-1} was due to the vibration of

carbonyl (C=O) group. Lastly, there were no peaks associated with vinyl C-H stretching (3000 – 3100 cm^{-1}), confirming complete polymerization of PFPMA monomer. Thin films of P(4VP-PFPMA) and P(4VP-PFPMA-DVB) (the latter containing 16.6% DVB, calculated using the peak area at 712 cm^{-1}] retained the characteristic absorptions of C=O stretching from the PFPMA units at 1776 cm^{-1} and the pyridine ring from the 4VP units (at 1597 cm^{-1}). Both peaks were marked with dashed lines in Figure 1a, confirming the successful copolymerization of 4VP and PFPMA through iCVD. The peak at 712 cm^{-1} (red arrow in Figure 1a), indicative of C-C vibration of the phenyl moieties in DVB,[52] was observed only in the spectrum of P(4VP-PFPMA-DVB). There was no peak observed at 903 cm^{-1}, the wavenumber indicative of unreacted/pendant vinyl bonds, hence confirming complete polymerization of P(4VP-PFPMA-DVB).[52] In addition, there was a slight shift observed for the C=O stretching peak, from 1780 cm^{-1} (for the PPFPMA homopolymer) to 1776 cm^{-1} (for the copolymers), indicating that the copolymerization reaction occurred rather than simple mixing of the homopolymers.

The wetting properties and stability of the as-deposited coatings were assessed using dynamic water contact angle measurements (Figure 2),[53] where advancing water contact angle reflects the surface energy under dry ambient conditions and receding water contact angle reflects that under submerged conditions. PPFPMA had an advancing contact angle of 98.6 ± 2.1° and receding contact angle of 83.0 ± 0.70°, indicating its moderate hydrophobicity with low hysteresis (i.e., 15.6°), which was consistent with previous reports.[54] P(4VP-PFPMA) and P(4VP-PFPMA-DVB) had advancing contact angles of 88.1 ± 4.3° and 92.4 ± 0.4°, and receding angles of 45.6 ± 5.2° and 47.0 ± 1.3°, hence contact angle hysteresis values of ~43° and ~45°, respectively. That large contact angle hysteresis was attributed to surface chain reorientation, which has been commonly observed on the surface of amphiphilic copolymers.[44] None of the

films tested demonstrated dissolution during the dynamic contact angle measurements, indicating good stability in an aqueous environment.

3.2 Vapor-phase derivatization to obtain copolymers containing pyridinium-based sulfobetaine

The derivatization, achieved by exposing the iCVD thin films to a vapor of PS, was done on P(4VP-PFPMA) and P(4VP-PFPMA-DVB). Distinct from previously reported derivatization temperature (i.e., 60°C), here a lower temperature of 40°C was used due to potential side reactions between PFPMA and PS. Indeed, when derivatized at 60°C, the PFPMA units in P(4VP-PFPMA) demonstrated a loss of the pentafluorophenyl groups, indicated by the reduced peak intensity at 1065 cm^{-1} and 995 cm^{-1} (corresponding to the ester bond and the C-F moiety, respectively), while the peaks at 1597 cm^{-1} and 1416 cm^{-1}, indicative of the 4VP units, remained unchanged (Figure S1). Furthermore, the peak corresponding to the SO_3^- group at 1205 cm^{-1} showed an increased area under the curve, implying replacement of the pentafluorophenyl group by the SO_3^- group at 60°C. That side reaction was minimized when the derivatization reaction was performed at 40°C, as indicated by the unchanged peak intensities for the pentafluorophenyl group before and after the reaction (Figure S1). To further prevent film dissolution after the vapor-phase derivatization, DVB was added to the copolymer. Successful derivatization of P(4VP-PFPMA-DVB) was confirmed by the new peak at 1643 cm^{-1}, which corresponded to a newly formed pyridinium ring, and the medium-strength peak at 1205 cm^{-1}, which corresponded to the symmetric vibration of SO_3^- group (Figure 1a).

Success of derivatization was further corroborated by XPS survey scans (Figure S2) and high-resolution N(1s) (Figure 1b) scans. The survey scans of P(4VP-PFPMA-DVB) and P(4VPz-PFPMA-DVB) demonstrated C at 287 eV, N at 401 eV, O at 535 eV and F at 690 eV. P(4VPz-

PFPMA-DVB) also had a S peak at 170 eV. The composition of P(4VP-PFPMA-DVB) was determined using the fluorine to nitrogen ratio and FTIR results for DVB composition in the coating (see Supporting Information), indicating a molar percentage of PFPMA of 37.7 ± 2.3%, which remained nearly unchanged (43.5 ± 5.6%) after the derivatization. Hence, the replacement of pentafluorophenyl group by SO_3^- group was minimal during the derivatization of P(4VP-PFPMA-DVB). The composition of about 56.5% 4VP and 43.5% PFPMA was chosen as a result of a series of composition optimization experiments, with the goal of obtaining a stable and insoluble hydrophilic coating to ensure good antifouling performance. As shown in Figure 2, hydrophobicity increased rapidly with higher amounts of PFPMA, which could jeopardize the antifouling properties of the coating. Meanwhile, incorporating more 4VP led to instability and dissolution of the coating after the enzyme immobilization reaction, as revealed by the XPS survey scans shown in Figure S3 and Table S1. It is worth noting that the content of S was 3-fold that of N, which can be attributed to the adsorption of unreacted PS on P(4VPz-PFPMA-DVB). For P(4VPz-PFPMA-DVB) with 21.8 ± 6.8% PFPMA, a significant reduction in fluorine (from 5.02% to 0.59%), sulfur (6.00 to 0.72%), a drastic increase in oxygen (from 14.04% to 26.93%) and presence of contaminant elements (i.e., a total of 12.83% of the elements of sodium, chlorine, and phosphorus, likely introduced by the contact with the PBS buffer) were observed after the enzyme immobilization reaction. The dissolution was most obvious from visual inspections using a digital microscope (Figure S4). Hence, P(4VPz-PFPMA-DVB) with 43.5 ± 5.6% PFPMA was used for subsequent enzyme immobilization and antifouling- antimicrobial performance evaluation.

In the N(1s) high-resolution spectra (Figure 1b), the formation of zwitterionic moieties led to a shift in the N(1s) binding energy, from 399.0 eV to 401.7 eV. The peaks before and after

the derivatization had no overlap, indicating complete conversion of pyridine to pyridinium at the surface of the P(4VP-PFPMA-DVB) thin film (XPS has a penetration depth of 10 nm).[55,56] Lastly, PPFPMA and P(4VPz-PFPMA-DVB) did not form any crystals as confirmed by XRD (Figure S5), following other perfluorinated monomers with short chain length.[57]

Wetting properties of the derivatized films were also assessed using dynamic water contact angle measurements (Figure 2). While the P(4VP-PFPMA-DVB) films demonstrated advancing and receding contact angles of 92.4 ± 0.4° and 47.0 ± 1.3°, the derivatized film, i.e., P(4VPz-PFPMA-DVB), had advancing and receding angles of 86.4 ± 2.2° and zero. The unchanged advancing contact angle confirmed that the derivatization did not remove a substantial amount of pentafluorophenyl side chains in PFPMA. The zero receding contact angle confirmed the hydrophilicity of the copolymer film when submerged, hinting at excellent antifouling properties. The large contact angle hysteresis was indicative of facile surface chain reorientations, as discussed above.[44]

In summary, FTIR, XPS, and dynamic contact angle measurements confirmed the successful synthesis of a novel zwitterionic copolymer, P(4VPz-PFPMA-DVB), which will be subject to the immobilization of lysozyme for the antimicrobial-antifouling dual function.

3.3 Enzyme immobilization on the zwitterionic copolymer via nucleophilic substitution

The nucleophilic substitution reaction, enabled by the pentafluorophenyl side groups in P(4VPz-PFPMA-DVB), allowed surface tethering of lysozyme via the primary amine groups in the enzyme. The primary amine groups in lysozyme can be divided into two classes: the α-amino group located at the N-terminus and the ε-amino groups introduced by lysine residues.[58] Therefore, during the bioconjugation step, both classes of primary amine groups could

participate in the nucleophilic substitution. Scheme 1 showed the reaction via α-amino group (at the N-terminus) only for illustration purposes.

The nucleophilic substitution reaction was performed by incubating the P(4VPz-PFPMA-DVB) thin films with 1 mg/mL solution of lysozyme dissolved in PBS for 6 hours at 37°C. Success of the bioconjugation was confirmed using XPS (Figure 3). Compositions of P(4VPz-PFPMA-DVB) and P(4VPz-PFPMA-DVB-lysozyme) were calculated from the XPS survey spectra (Figure 3a) and summarized in Table 2. Upon completion of the bioconjugation step, the atomic percentage of nitrogen increased from 1.50% [for P(4VPz-PFPMA-DVB)] to 4.39% P(4VPz-PFPMA-DVB-lysozyme) due to the tethering of lysozymes (which has an atomic percentage of nitrogen of 17.40%). Additionally, the amount of sulfur changed from 3.80% to 3.00% after the immobilization reaction due to presence of lysozyme (which has an atomic percentage of sulfur of 1.10%). The atomic percentage of fluorine decreased from 9.87% [for P(4VPz-PFPMA-DVB)] to 7.17% [P(4VPz-PFPMA-DVB-lysozyme)], indicating replacement of the pentafluorophenyl group by lysozyme (Scheme 1). That change in fluorine content corresponded to a degree of substitution of 27.4%, i.e., 27.4% of the PFPMA moieties in P(4VPz-PFPMA-DVB) were converted to immobilization sites for lysozyme. That represents the highest degree of substitution that we were able to achieve, based on extensive optimization experiments around the reaction conditions (e.g., temperature and duration). Furthermore, high-resolution N(1s) scans illustrated that a new peak at 399.7 eV emerged in the spectrum for P(4VPz-PFPMA-DVB-lysozyme) compared to that for P(4VPz-PFPMA-DVB), corresponding to the amide bond introduced by the surface-immobilized lysozyme.[59] The peak corresponding to the pyridinium nitrogen, at 401.7 eV, was retained. Hence, XPS confirmed that lysozyme was

immobilized onto P(4VPz-PFPMA-DVB) via nucleophilic substitution of the pentafluorophenyl group, while retaining the zwitterionic moieties in the copolymer thin films.

Presence of the surface-tethered lysozymes was further confirmed via morphological characterizations using AFM and SEM and comparison to the morphology of PPFPMA, P4VP, and P(4VPz-PFPMA-DVB) thin films (Figure 4). The homopolymer of PPFPMA (with the thickness of 242.6 ± 25.3 nm) demonstrated a root-mean-square (RMS) roughness of 37.29 ± 10.53 nm (Figure 4a), which was in agreement with previous studies.[60,61] This high roughness could be attributed to cluster formation during iCVD polymerization due to the strong intermolecular interactions of PFPMA monomers.[41] The homopolymer of P4VP (with the thickness of 236.3 ± 8.6 nm) was extremely smooth with the RMS roughness of 0.53 ± 0.10 nm (Figure 4b), which was consistent with the RMS roughness of most iCVD polymer thin films.[35] Similarly, P(4VPz -PFPMA-DVB) copolymer thin films (with the thickness of 271.5 ± 8.9 nm) demonstrated a similar RMS roughness of 0.69 ± 0.18 nm (Figure 4c). The thin film of P(4VPz -PFPMA-DVB-lysozyme) had an RMS roughness of 2.66 ± 1.48 nm (Figure 4d), about 5-fold the roughness of P(4VPz -PFPMA-DVB). This increment in roughness was a result of the successful attachment of lysozymes onto the surface of the film, as evident from the morphology captured in the AFM image (Figure 4d). The morphology of lysozyme clusters on the surface of P(4VPz -PFPMA-DVB-lysozyme) was also confirmed using SEM. The thin film of P(4VPz-PFPMA-DVB) was smooth and free of surface defects (Figure 4e), whereas protein aggregates emerged after the nucleophilic substitution reaction (Figure 4f) [See Figure S6 for lower magnification images]. The average diameter of the aggregates on the P(4VPz -PFPMA-DVB-lysozyme), as measured using the SEM images, was 37.8 ± 31.6 nm (n=3, typical diameter of lysozyme is 1.5-6 nm),[62] which agreed well with previous studies.[63]

3.4 Antifouling-antimicrobial dual function achieved by P(4VPz -PFPMA-DVB-lysozyme)

Polymers containing pyridinium-based sulfobetaine are well known for their excellent antifouling performance.[44] Nevertheless, the extreme hydrophilicity of sulfobetaine groups sometimes render the polymer thin film soluble during prolonged incubation in aqueous environments.[64] To confirm that the coatings were not water-soluble and was sufficiently stable for the antifouling/antimicrobial assessments, P(4VPz-PFPMA-DVB) and P(4VPz-PFPMA-DVB-lysozyme) were incubated in LB medium at 37°C for 8 hours. The coating thickness of P(4VPz-PFPMA-DVB) remained unchanged after the incubation (Figure S7), confirming the insolubility of the coating. We were not able to quantify the thickness of P(4VPz-PFPMA-DVB-lysozyme) after the incubation due to its high surface roughness and large error in the ellipsometry measurements, which was likely a result of the conformational change of the surface-attached lysozyme. As such, we instead used FTIR to assess the chemical stability of P(4VPz-PFPMA-DVB-lysozyme) (Figure S8). In the FTIR spectra before and after incubation. the peaks at 1775 cm^{-1} (C=O group), 1641 cm^{-1} (quaternized pyridinium ring), and 1209 cm^{-1} (SO_3^- group) remained unchanged, indicating minimal change in the coating composition after the incubation.

The antifouling-antimicrobial dual function was assessed by incubating P(4VPz-PFPMA-DVB-lysozyme), P(4VPz-PFPMA-DVB), and PVC (the latter two for the purpose of comparison) in concentrated cultures of *P. aeruginosa* (gram-negative) or *B. subtilis* (gram-negative) for 2 hours, followed by staining using the LIVE/DEAD BacLight Bacterial Viability Kit and imaging using confocal microscopy. The 2-hour incubation was select to avoid formation of biofilm on the PVC surface (which was most prone to biofouling) and to ensure that the adhesion/eradication of bacteria on the surfaces was fully quantifiable. Antifouling performance

was quantified by dividing the total number of surface-attached bacteria on P(4VPz-PFPMA-DVB-lysozyme) [or P(4VPz-PFPMA-DVB)] by that on a PVC surface, while antimicrobial performance was quantified by dividing the number of dead cells on each surface by the total number of cells (both alive and dead) on that surface. PVC was chosen as a benchmark for an "uncoated" surface because it is commonly used in microbiology studies as the material for culture plates.[23]

The antifouling performance was assessed using a gram-negative bacterium, *P. aeruginosa* strain PAO1, due to its strong tendency to form biofilms and cause severe fouling on submerged surfaces.[44] Figure 5a shows the fluorescent confocal images of *P. aeruginosa* on PVC, P(4VPz-PFPMA-DVB), and P(4VPz-PFPMA-DVB-lysozyme). As expected, the greatest amount of *P. aeruginosa* was captured on the surface of PVC. The counts of bacteria on P(4VPz-PFPMA-DVB) were 26 ± 2% (n = 5) the bacterial counts on PVC, indicating good antifouling performance of this copolymer. Interestingly, P(4VPz-PFPMA-DVB-lysozyme) achieved even better antifouling performance, with a reduction of 87 ± 12% (n = 5) compared to PVC. Similar observations, namely enhanced antifouling performance upon incorporation of lysozymes, have been previously reported for poly(ethylene glycol)[65], and poly(ethylene glycol methacrylate) coatings,[66] albeit the underlying mechanism for this enhancement remains elusive. Although this was the first time that lysozyme has been incorporated into zwitterionic thin films, we hypothesize that the observed reduction in bacterial adhesion was due to the inherent fouling resistance of lysozyme, which displays a hydrophilic surface[67,68] with most nonpolar groups buried in cavities.[69] This hypothesis was corroborated by the dynamic water contact angles measured on P(4VPz-PFPMA-DVB-lysozyme). According to Figure 2, the advancing contact angle of P(4VPz-PFPMA-DVB-lysozyme) was 57.5 ± 3.1°, which was ~ 30° lower than the

advancing water contact angle of (P4VPz-PFPMA-DVB). Such significant reduction was attributed to the hydrophilicity of lysozymes. That hydrophilic protein surface could increase the enthalpic barrier to bacterial adhesion. Hence, we attributed the further reduction of bacterial adhesion on dual function coatings to the higher concentration of polar groups at the surface of lysozyme. Dead cells (indicated by red fluorescence) were absent from all three surfaces, including P(4VPz-PFPMA-DVB-lysozyme), which was consistent with the literature reporting that the antimicrobial effects of lysozyme target gram-positive bacteria.[70]

To assess that antimicrobial effect against gram-positive bacteria, *B. subtilis* strain DK1042 was used as a second model strain (Figure 5b). A lower number of *B. subtilis* cells adhered to PVC compared to the number of adhered *P. aeruginosa* due to the well-characterized biofilm-forming tendency of the latter. Nevertheless, similar to the antifouling performance against *P. aeruginosa,* P(4VPz-PFPMA-DVB) also led to a fouling reduction of 71 ± 13% (n =5) against *B. subtilis*, compared to that on PVC. P(4VPz-PFPMA-DVB-lysozyme) demonstrated antifouling-antimicrobial dual function, where the total cell count of *B. subtilis* was reduced by 75 ± 14% (n = 5) compared to that on PVC and 67 ± 2% (n = 5) of the adhered cells were deactivated (indicated by red fluorescence). We believe that achieving the highest possible degree of substitution for the enzyme immobilization is critical for the antimicrobial performance and that the deactivation rate of 67 ± 2% was the maximum antimicrobial effect achievable using the reported copolymer system.

3.5 Cytotoxicity of P(4VPz -PFPMA-DVB-lysozyme)

Cytotoxicity of P(4VPz-PFPMA-DVB-lysozyme) was evaluated and quantified with the HDF cells, a connective tissue cell line commonly used to assess cell viability after exposing to potentially cytotoxic compounds. Cell viability after the exposure was quantified by using the

CCK-8 assay. The percentage of cell viability was assessed with pristine cover slips, which served as the control group, and with P(4VPz-PFPMA-DVB-lysozyme)-coated cover slips as the testing group for 24 and 48 hours (Figure 6).

Reduction in the average cell viability was observed after 24- and 48-hour incubations with statistical significance ($p < 0.05$). Specifically, the average cell viability on P(4VPz-PFPMA-DVB-lysozyme)-coated cover slips was 86.0 ± 0.2% after 24 hours of incubation and 73.7 ± 1.1%, after 48 hours of incubation, compared to the cell viability on pristine cover slips. Those reductions in cell viability could be attributed to the presence of fluorine elements in the coating (with an atomic percentage of ~7.17%). Fluorine-containing compounds have been reported to inhibit mammalian cell growth.[71] Nevertheless, we determined that this cytotoxicity is slight to mild, based on the ISO 10993-5 international standard, which indicates that *in vitro* cell viability above 70% is considered acceptable for applications in medical devices. As such, P(4VPz-PFPMA-DVB-lysozyme) could serve as effective antimicrobial coatings in a broad range of medical and sustainability applications.[72–74] To further reduce the cytotoxicity, the remaining PFPMA units in the P(4VPz-PFPMA-DVB-lysozyme) could be eliminated through a subsequent reaction with 2-(2-aminoethoxy)ethanol, as shown in previous reports.[40]

4. Conclusion

In conclusion, we demonstrated a three-step procedure to synthesize a novel bioconjugated zwitterionic coating with antifouling-antimicrobial dual function. The three steps comprised (1) vapor-deposition of the copolymer P(4VP-PFPMA-DVB), affording pyridine nitrogen, (2) low-temperature and all-dry derivatization of the pyridine nitrogen (via exposure to PS) to form pyridinium-based zwitterionic moieties, and (3) immobilization of an antimicrobial

enzyme, lysozyme, via nucleophilic substitution of the pentafluorophenyl group. The simultaneous antifouling and antimicrobial functions of the novel material, P(4VPz-PFPMA-DVB-lysozyme), was illustrated by a reduction of 87 ± 12 % in the adhesion of a biofilm-forming strain (PAO1) compared to uncoated PVC and a reduction of 75 ± 16% in the adhesion of *B. subtilis*. The immobilized lysozyme was antimicrobial against the gram-positive bacterium, *B. subtilis,* deactivating 67 ± 2% of the adhered cells. Based on the reduction of adhesion by gram-negative bacteria and the deactivation of gram-positive bacteria, P(4VPz-PFPMA-DVB-lysozyme*)* represents a promising biomaterial. Despite the mild reduction in the viability of the HDF cells grown on P(4VPz-PFPMA-DVB-lysozyme) (i.e., 73.7 ± 1.1%)*,* this level of cytotoxicity remains within acceptable range for biomedical applications. Therefore, we concluded that that P(4VPz-PFPMA-DVB-lysozyme) could reduce the transmission of infectious diseases in the healthcare and public facilities with incurring mild toxicity. Although not a focus of the current study, the residual PFPMA units in the copolymer could be removed through a secondary reaction with 2-(2-aminoethoxy)ethanol, to further improve biocompatibility of the coating for potential *in vivo* applications.[40] Future studies will also focus on the detailed evaluations of the effect of surface-immobilization on enzymatic activity, stability, protein structure, and the long-term effectiveness of the novel coating. The degree of substitution of pentafluorophenyl group by the enzyme immobilization reaction will be optimized by systematically varying the reaction conditions.

5. Conflicts of interest

There are no conflicts to declare.

6. Acknowledgements

This research was funded by the National Institutes of Health under the award NIHDC016644, and the Department of Navy Office of Naval Research (ONR) grant N00014-20-1-2418. AK is supported by the Samuel C. Fleming Family Graduate Fellowship. This work made use of the Cornell Center for Materials Research (CCMR) Shared Facilities, which are funded through the NSF MRSEC program (DMR-1719875), and Cornell University Biotechnology Resource Center, that is funded by NIH (S10RR025502). The authors thank Pengyu Chen for assistance with culturing *Bacillus subtilis.*

7. References

1 Z. K. Zander and M. L. Becker, *ACS Macro Letters*, 2018, **7**, 16–25.

2 L. Mi and S. Jiang, *Angewandte Chemie - International Edition*, 2014, 53, 1746–1754.

3 S. Vigneswari, T. S. M. Amelia, M. H. Hazwan, G. K. Mouriya, K. Bhubalan, A. A. A. Amirul and S. Ramakrishna, *Antibiotics*, 2021, **10**, 1–22.

4 T. P. Martin, S. E. Kooi, S. H. Chang, K. L. Sedransk and K. K. Gleason, *Biomaterials*, 2007, **28**, 909–915.

5 X. Ren, L. Kou, H. B. Kocer, C. Zhu, S. D. Worley, R. M. Broughton and T. S. Huang, *Colloids and Surfaces A: Physicochemical and Engineering Aspects*, 2008, **317**, 711–716.

6 G. Lesnierowski and J. Kijowski, in *Bioactive Egg Compounds*, Springer-Verlag, 2007, pp. 33–42.

7 V. Muriel-Galet, J. N. Talbert, P. Hernandez-Munoz, R. Gavara and J. M. Goddard, *Journal of Agricultural and Food Chemistry*, 2013, **61**, 6720–6727.

8 P. Bayazidi, H. Almasi and A. K. Asl, *International Journal of Biological Macromolecules*, 2018, **107**, 2544–2551.

9 W. Lee, S. K. Ku, D. H. Na and J. S. Bae, *Inflammation*, 2015, **38**, 1911–1924.

10 J. K. Mann and T. Ndung'u, *Future Virology*, 2020, 15, 609–624.

11 J. Małaczewska, E. Kaczorek-ŁUkowska, R. Wójcik and A. Krzysztof Siwicki, *BMC Veterinary Research*, 2019, **15**, 318.

12 C. Su, Y. Hu, Q. Song, Y. Ye, L. Gao, P. Li and T. Ye, *ACS Applied Materials and Interfaces*, 2020, **12**, 18978–18986.

13 Q. Zeng, Y. Zhu, B. Yu, Y. Sun, X. Ding, C. Xu, Y. W. Wu, Z. Tang and F. J. Xu, *Biomacromolecules*, 2018, **19**, 2805–2811.

14 A. Vaishampayan, A. de Jong, D. J. Wight, J. Kok and E. Grohmann, *Frontiers in Microbiology*, 2018, **9**, 221.

15 T. B. Donadt and R. Yang, *ACS Biomaterials Science and Engineering*, 2020, **6**, 182–197.

16 Q. Shao and S. Jiang, *Advanced Materials*, 2015, **27**, 15–26.

17 J. Du, Y. Tang, A. L. Lewis and S. P. Armes, *Journal of the American Chemical Society*, 2005, **127**, 17982–17983.

18 A. B. Lowe and C. L. McCormick, *Chemical Reviews*, 2002, **102**, 4177–4189.

19 L. Zheng, H. S. Sundaram, Z. Wei, C. Li and Z. Yuan, *Reactive and Functional Polymers*, 2017, 118, 51–61.

20 S. Jiang and Z. Cao, *Advanced Materials*, 2010, **22**, 920–932.

21 J. Wu, W. Lin, Z. Wang, S. Chen and Y. Chang, *Langmuir*, 2012, **28**, 7436–7441.

22 L. D. Blackman, P. A. Gunatillake, P. Cass and K. E. S. Locock, *Chemical Society Reviews*, 2019, 48, 757–770.

23 P. Chen, J. Lang, T. Donadt, Z. Yu and R. Yang, *ACS Biomaterials Science and Engineering*, , DOI:10.1021/acsbiomaterials.0c01691.

24 F. Zaccarian, M. B. Baker and M. J. Webber, *Organic Materials*, 2020, **02**, 342–357.

25 Q. Jin, Y. Chen, Y. Wang and J. Ji, *Colloids and Surfaces B: Biointerfaces*, 2014, **124**, 80–86.

26 L. Zhang, Z. Cao, T. Bai, L. Carr, J. R. Ella-Menye, C. Irvin, B. D. Ratner and S. Jiang, *Nature Biotechnology*, 2013, **31**, 553–556.

27 C. Zhang, X. Dong, Z. Guo and Y. Sun, *Journal of Colloid and Interface Science*, 2018, **519**, 145–153.

28 A. Khlyustova, Y. Cheng and R. Yang, *Journal of Materials Chemistry B*, 2020, 8, 6588–6609.

29 U. Capasso Palmiero, M. Maraldi, N. Manfredini and D. Moscatelli, *Biomacromolecules*, 2018, **19**, 1314–1323.

30 G. Cheng, Z. Zhang, S. Chen, J. D. Bryers and S. Jiang, *Biomaterials*, 2007, **28**, 4192–4199.

31 Q. Yu, Z. Wu and H. Chen, *Acta Biomaterialia*, 2015, 16, 1–13.

32 H. D. M. Follmann, A. F. Martins, A. P. Gerola, T. A. L. Burgo, C. v. Nakamura, A. F. Rubira and E. C. Muniz, *Biomacromolecules*, 2012, **13**, 3711–3722.

33 Z. Cao, N. Brault, H. Xue, A. Keefe and S. Jiang, *Angewandte Chemie - International Edition*, 2011, **50**, 6102–6104.

34 Z. Cao, L. Mi, J. Mendiola, J. R. Ella-Menye, L. Zhang, H. Xue and S. Jiang, *Angewandte Chemie - International Edition*, 2012, **51**, 2602–2605.

35 R. Yang, J. Xu, G. Ozaydin-Ince, S. Y. Wong and K. K. Gleason, *Chemistry of Materials*, 2011, **23**, 1263–1272.

36 A. Asatekin, M. C. Barr, S. H. Baxamusa, K. K. S. Lau, W. Tenhaeff, J. Xu and K. K. Gleason, *Materials Today*, 2010, **13**, 26–33.

37 H. Z. Shafi, M. Wang, K. K. Gleason and Z. Khan, *Materials Chemistry and Physics*, 2020, **239**, 121971.

38 W. S. O'Shaughnessy, M. Gao and K. K. Gleason, *Langmuir*, 2006, **22**, 7021–7026.

39 R. Bakker, V. Verlaan, C. H. M. van der Werf, J. K. Rath, K. K. Gleason and R. E. I. Schropp, *Surface and Coatings Technology*, 2007, **201**, 9422–9425.

40 N. Marí-Buyé, S. O'Shaughnessy, C. Colominas, C. E. Semino, K. K. Gleason and S. Borrós, *Advanced Functional Materials*, 2009, **19**, 1276–1286.

41 A. Cifuentes and S. Borrós, *Langmuir*, 2013, **29**, 6645–6651.

42 H. Z. Shafi, Z. Khan, R. Yang and K. K. Gleason, *Desalination*, 2015, **362**, 93–103.

43 A. Khlyustova and R. Yang, *Frontiers in Bioengineering and Biotechnology*, 2021, **9**, 670541.

44 T. B. Donadt and R. Yang, *Advanced Materials Interfaces*, 2021, **8**, 2001791.

45 R. Yang, H. Jang, R. Stocker and K. K. Gleason, *Advanced Materials*, 2014, **26**, 1711–1718.

46 M. Muller Dos Santos, A. Souza Da Rosa, S. Dal'Boit, D. A. Mitchell and N. Krieger, *Bioresource Technology*, 2004, **93**, 261–268.

47 J. Xu and K. K. Gleason, *Chemistry of Materials*, 2010, **22**, 1732–1738.

48 S. J. P. McInnes, E. J. Szili, S. A. Al-Bataineh, J. Xu, M. E. Alf, K. K. Gleason, R. D. Short and N. H. Voelcker, *ACS Applied Materials and Interfaces*, 2012, **4**, 3566–3574.

49 E. Mhatre, A. Sundaram, T. Hölscher, M. Mühlstädt, J. Bossert and Á. T. Kovács, *Microorganisms*, 2017, **5**, 7.

50 K. K. S. Lau and K. K. Gleason, *Macromolecules*, 2006, **39**, 3695–3703.

51 K. K. S. Lau and K. K. Gleason, *Macromolecules*, 2006, **39**, 3688–3694.

52 C. D. Petruczok, R. Yang and K. K. Gleason, *Macromolecules*, 2013, **46**, 1832–1840.

53 T. Huhtamäki, X. Tian, J. T. Korhonen and R. H. A. Ras, *Nature Protocols*, 2018, **13**, 1521–1538.

54 K. A. Günay, N. Schüwer and H. A. Klok, *Polymer Chemistry*, 2012, **3**, 2186–2192.

55 Z. Zhao, F. Liu, L. Zhao and S. Yan, *Applied Physics A: Materials Science and Processing*, 2011, **103**, 1059–1065.

56 A. Zuber, A. Bachhuka, S. Tassios, C. Tiddy, K. Vasilev and H. Ebendorff-Heidepriem, *Sensors (Switzerland)*, 2020, **20**, 492.
57 A. Liu, E. Goktekin and K. K. Gleason, *Langmuir*, 2014, **30**, 14189–14194.
58 O. Koniev and A. Wagner, *Chemical Society Reviews*, 2015, **44**, 5495–5551.
59 L. Francesch, S. Borros, W. Knoll and R. Förch, *Langmuir*, 2007, **23**, 3927–3931.
60 A. Cifuentes, L. Masramon, A. Planas and S. Borrós, in *International Symposium on Plasma Chemistry*, 2011.
61 L. Duque, B. Menges, S. Borros and R. Förch, *Biomacromolecules*, 2010, **11**, 2818–2823.
62 G. Yang, C. Cecconi, W. A. Baase, I. R. Vetter, W. A. Breyer, J. A. Haack, B. W. Matthews, F. W. Dahlquist and C. Bustamante, *PNAS*, 2000, **97**, 139–144.
63 B. Wang, Q. Lin, T. Jin, C. Shen, J. Tang, Y. Han and H. Chen, *RSC Advances*, 2015, **5**, 3597–3604.
64 L. Kisley, K. A. Miller, C. M. Davis, D. Guin, E. A. Murphy, M. Gruebele and D. E. Leckband, *Biomacromolecules*, 2018, **19**, 3894–3901.
65 A. Caro, V. Humblot, C. Méthivier, M. Minier, M. Salmain and C. M. Pradier, *Journal of Physical Chemistry B*, 2009, **113**, 2101–2109.
66 S. Yuan, D. Wan, B. Liang, S. O. Pehkonen, Y. P. Ting, K. G. Neoh and E. T. Kang, *Langmuir*, 2011, **27**, 2761–2774.
67 C. C. F. Blake, D. F. Koenig, G. A. Mair, A. C. T. North, D. C. Phillips and V. R. Sarma, *Nature*, 1965, **4986**, 757–761.
68 K. Theis, Hen Egg-White (HEW) Lysozyme, https://proteopedia.org/wiki/index.php/Hen_Egg-White_(HEW)_Lysozyme, (accessed December 26, 2021).
69 M. Jafari and F. Mehrnejad, *PLoS ONE*, 2016, **11**, 0165213.
70 B. Masschalck, D. Deckers and C. W. Michiels, *Journal of Food Protection*, 2002, **65**, 1916–1923.
71 Y.-C. Chang and M.-Y. Chou, *Oral Surgery, Oral Medicine, Oral Pathology, Oral Radiology, and Endodontology*, 2001, **91**, 230–234.
72 M. R. Romano, M. Ferrara, C. Gatto, B. Ferrari, L. Giurgola and J. D. Tóthová, *Translational Vision Science and Technology*, 2019, **8**, 24.
73 *ISO 10993-5. Biological evaluation of medical devices. Part 5: Tests for in vitro cytotoxicity*, 2009.
74 L. Rodríguez-López, A. López-Prieto, M. Lopez-Álvarez, S. Pérez-Davila, J. Serra, P. González, J. M. Cruz and A. B. Moldes, *ACS Omega*, 2020, **5**, 31381–31390.
75 K. S. Siow, L. Britcher, S. Kumar and H. J. Griesser, *Colloids and Surfaces B: Biointerfaces*, 2019, **173**, 447–453.
76 RCSB Protein Data Bank, https://www.rcsb.org/, (accessed November 20, 2021).

8. Tables

Table 1. iCVD deposition conditions of the polymer thin films.

Sample	Flow rate (sccm)					Stage Temperature (°C)
	4VP	PFPMA	DVB	Argon	TBPO	
PPFPMA		0.22 ± 0.03			0.51 ± 0.04	32.5 ± 2.6
P4VP	2.28 ± 0.02			1.99 ± 0.05	1.01 ± 0.03	27.2 ± 1.3
P(4VP-PFPMA)	1.01 ± 0.06	0.25 ± 0.06		0.25 ± 0.06	0.51 ± 0.07	30.7 ± 1.6
P(4VP-PFPMA-DVB)	1.10 ± 0.05	0.23 ± 0.02	0.20 ± 0.01		0.49 ± 0.02	30.3 ± 3.6

Table 2. Elemental compositions of P(4VPz-PFPMA-DVB) with 43.5 ± 5.6% PFPMA before and after the enzyme immobilization step, derived from their XPS survey scans, and the theoretical elemental composition of lysozyme.[75]

Sample	O %	C %	N %	F %	S %
P(4VP-PFPMA-DVB)	5.70	79.99	2.62	11.68	
P(4VPz-PFPMA-DVB)	12.42	71.92	1.50	9.87	3.80
P(4VPz-PFPMA-DVB-lysozyme)	13.15	72.29	4.39	7.17	3.00
Lysozyme	19.90	61.70	17.40		1.10

9. Schemes

Scheme 1. Schematic of (a) the copolymerization reaction to produce P(4VP-PFPMA-DVB) via iCVD, and the subsequent treatment to produce zwitterionic moieties; (b) nucleophilic substitution reaction for enzyme immobilization. The 3D structure of lysozyme was obtained from RCSB Protein Data Bank.[76] Note that other primary amines in lysozyme likely also react with the polymer and here the N-terminus was used only for illustration purposes.

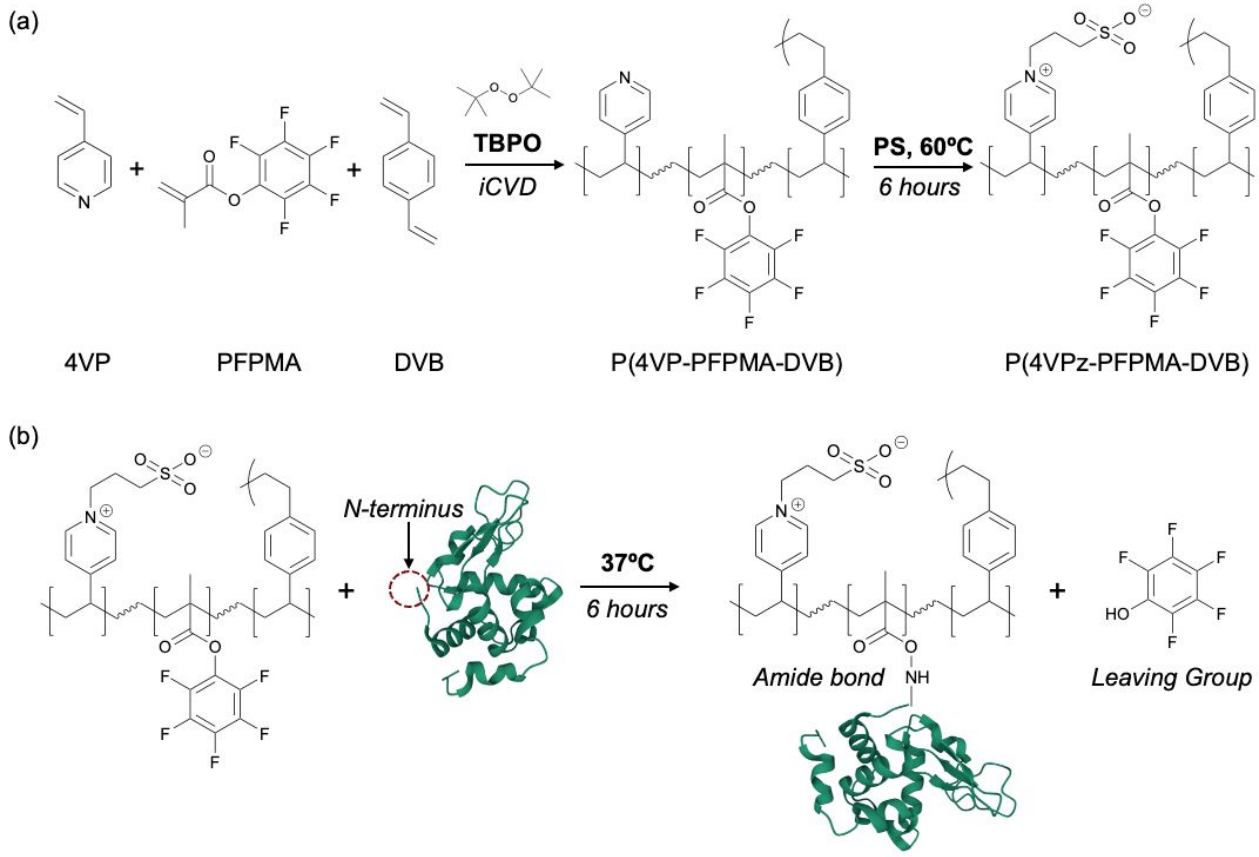

10. Figures

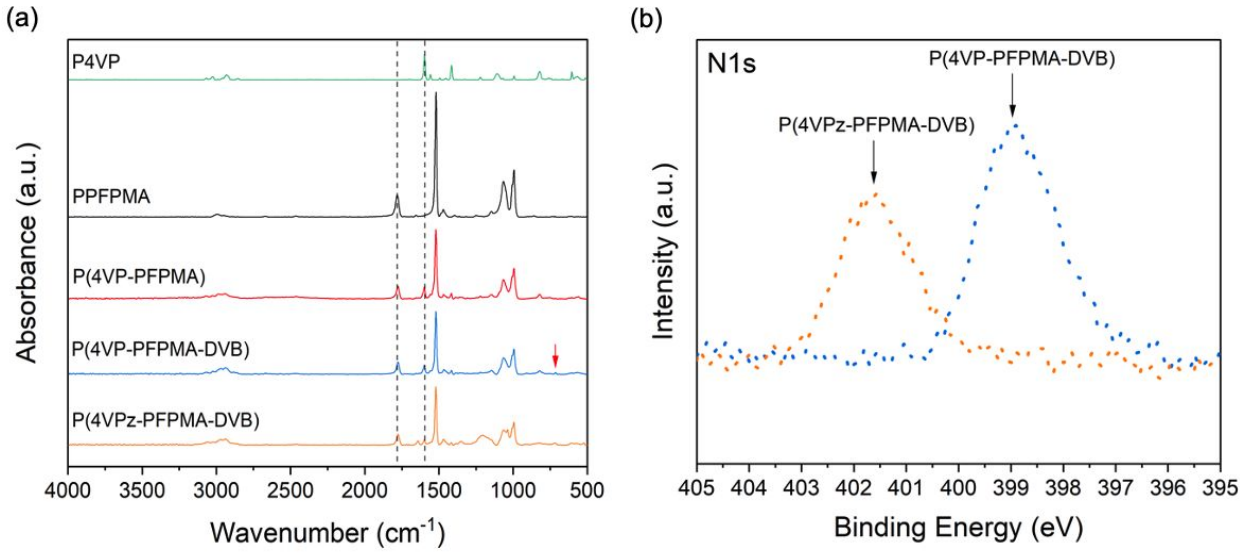

Figure 1. Chemical characterization of the polymer thin films deposited by iCVD. (a) FTIR spectra of the homopolymers, P4VP and PPFPMA, as well as copolymers, P(4VP-PFPMA), P(4VP-PFPMA-DVB) and P(4VPz-PFPMA-DVB). The red arrow indicates the characteristic peak for DVB, located at 712 cm^{-1}. The dashed lines represent the peaks attributed to the carbonyl group at 1776 cm^{-1} and the pyridinium ring at 1597 cm^{-1}. (b) XPS N(1s) high-resolution spectra for P(4VP-PFPMA-DVB) and its zwitterionic derivative, P(4VPz-PFPMA-DVB).

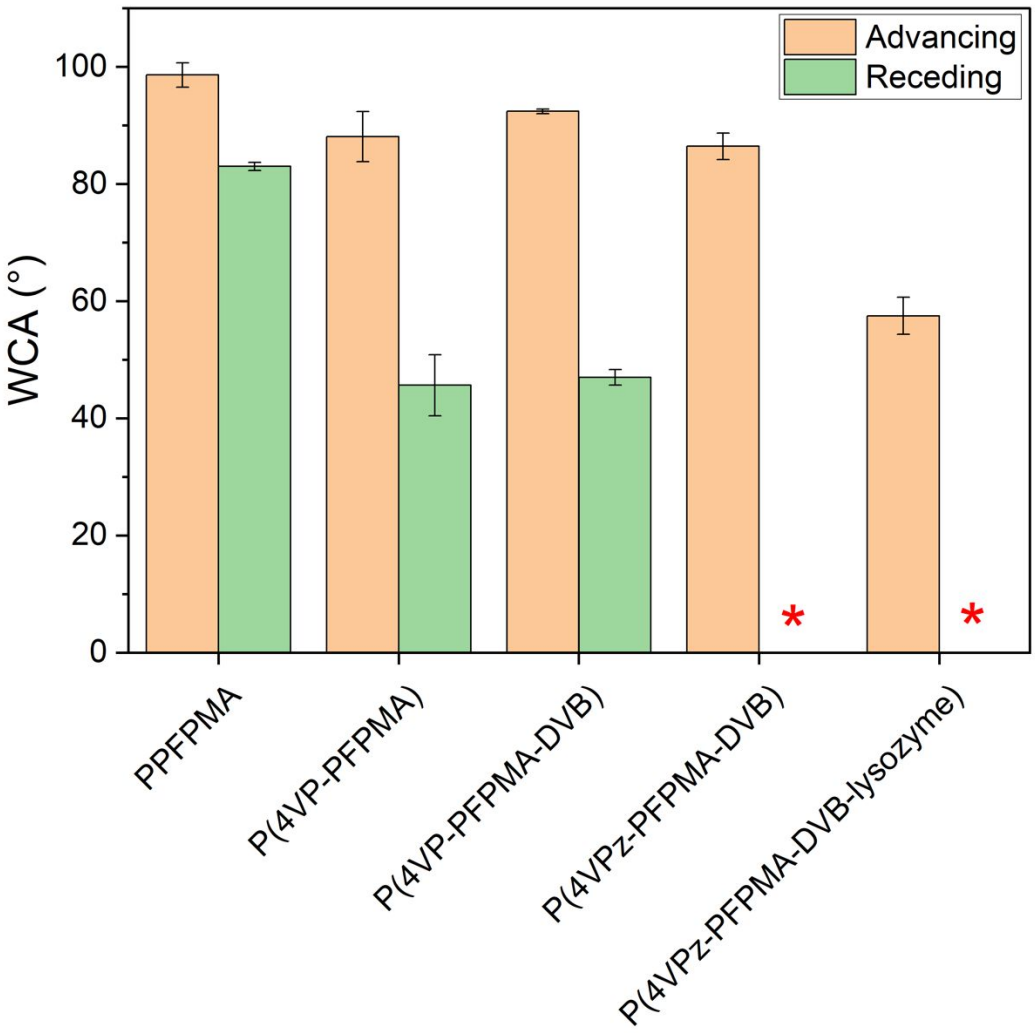

Figure 2. Dynamic water contact angle measurements for PPFPMA homopolymer, P(4VP-PFPMA), P(4VP-PFPMA-DVB) and P(4VPz-PFPMA-DVB) copolymer thin films. Note that the receding contact angles of P(4VPz-PFPMA-DVB) and P(4VPz-PFPMA-DVB-lysozyme) were zero (marked with red asterisks).

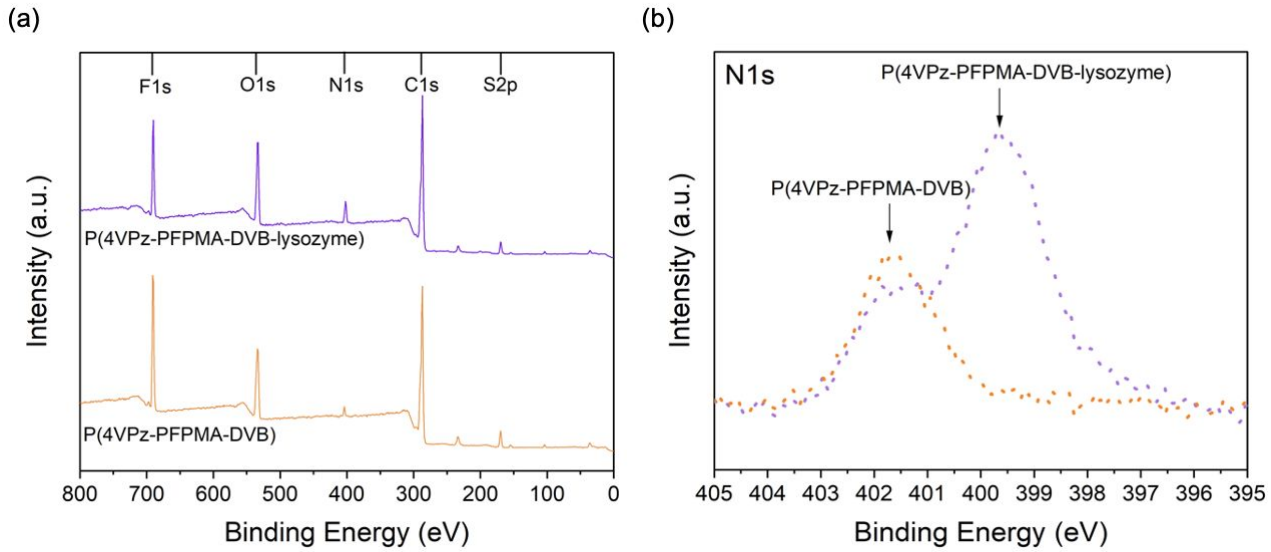

683
684 **Figure 3.** XPS (a) survey scans and (b) high-resolution N(1s) spectra of P(4VPz-PFPMA-DVB)
685 with 43.5 ± 5.6% PFPMA before and after the enzyme immobilization. The peaks at 233 eV and
686 170 eV correspond to S2s and S2p, respectively.

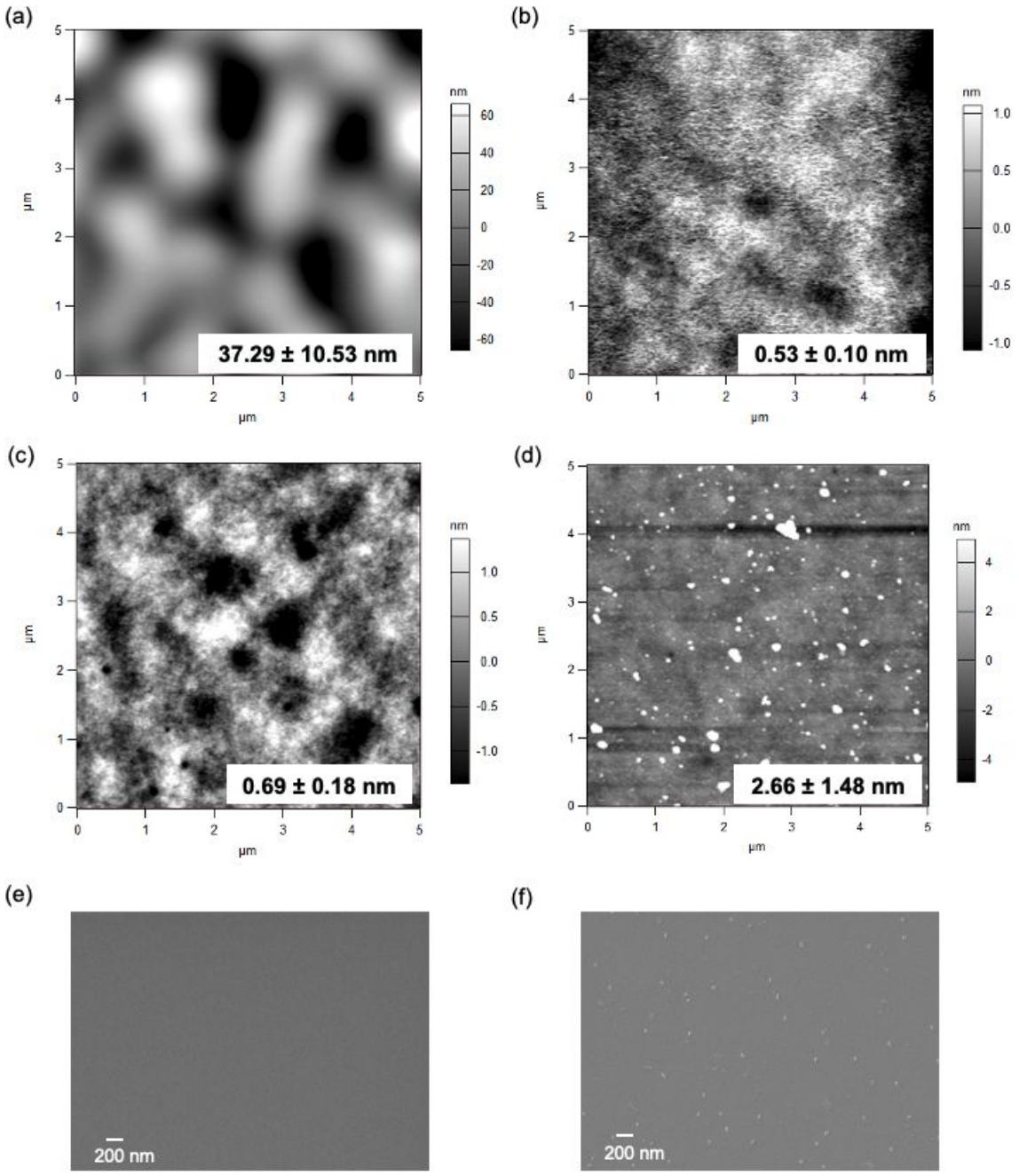

Figure 4. Topographical and morphological characterization of the polymer thin films. AFM images with respective RMS surface roughness of iCVD-synthesized (a) PPFPMA homopolymer, (b) P4VP homopolymer, (c) P(4VPz-PFPMA-DVB) thin film, and (d) P(4VPz-PFPMA-DVB-lysozyme) thin film. Data = Mean ± SD, n=2. SEM images of P(4VPz-PFPMA-DVB) (e) before and (f) after the enzyme immobilization reaction.

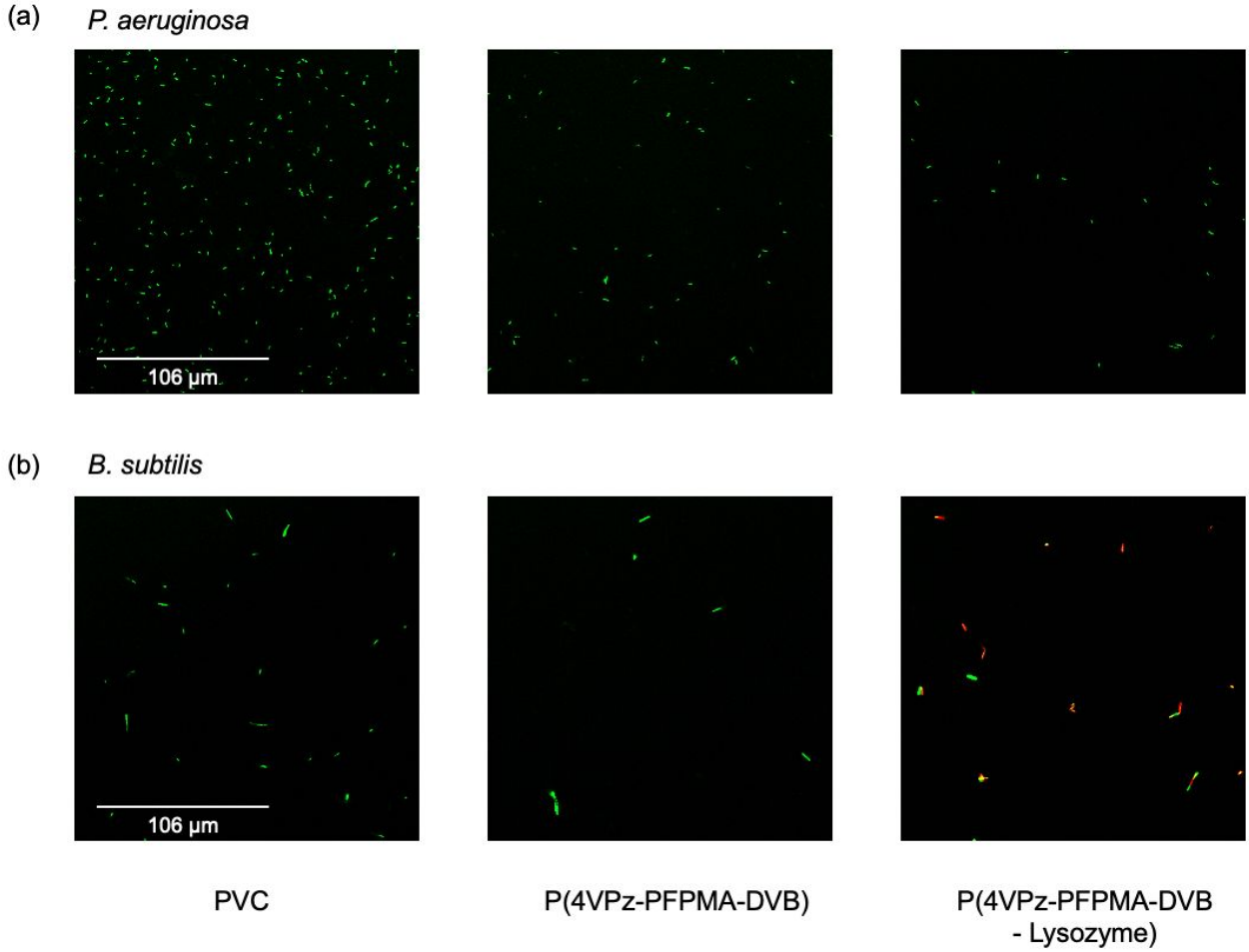

Figure 5. Confocal microscope images of (a) *P. aeruginosa* and (b) *B. subtilis* after a 2-hour incubation at 37°C with PVC films, P(4VPz-PFPMA-DVB), and P(4VPz-PFPMA-DVB-lysozyme). All images were taken with the same magnification.

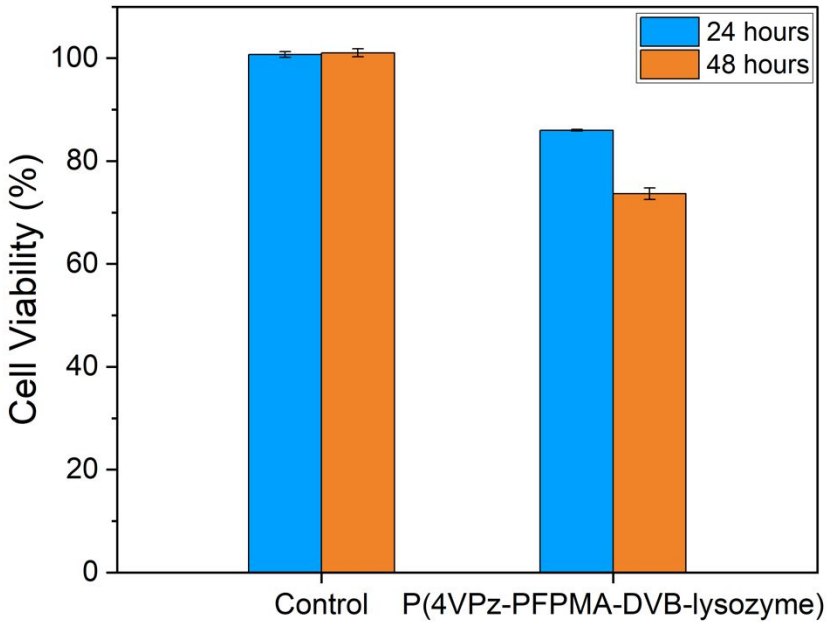

Figure 6. Cytotoxicity results for HDF cells, after co-incubating with P(4VPz-PFPMA-DVB-lysozyme) or pristine cover slips (i.e., "Control"), for 24 and 48 hours.